Flame-wall interaction modelling for pre-chamber combustion in lean burn gas engines

I. Hernández[1], E, Shapiro[2], N. Tiney[2], M. Kotzagianni[3], P. Kyrtatos[3], K. Boulouchos[3]

1. Ricardo Prague s.r.o., Prague Technical Centre, Palác Karlín, Thámova 11-13, Praha 8, 186 00, Czech Republic

2. Ricardo UK, Shoreham Technical Centre, Shoreham by Sea, BN43 5FG, UK

3. ETH Zürich, Department of Mechanical and Process Engineering, Sonneggstrasse 3, 8092 Zürich, Switzerland

Email: **ignacio.hernandez@ricardo.com**

Web: **www.ricardo.com**

Summary

Lean burn combustion systems present a viable route to emissions reductions. Scavenged pre-chamber ignition (PCI) systems aim to address this challenge by creating favourable ignition conditions close to stoichiometry in the spark region. The lean main charge ignition is then delivered by flame jets propagating through the nozzles connecting the pre-chamber to the cylinder. However, when using pre-chambers in light-duty applications, several problems need to be overcome compared to conventional ignition systems.

The interaction of the flame with the walls of the pre-chamber is an important issue affecting operation of the PCI combustion system. The flame may quench near to the wall due to heat losses. This is more prominent in PCIs designed for light-duty vehicles as the characteristic size of PCIs can be comparable with the flame quenching distance. Near wall quenching also affects the quality of the fuel mixture within the pre-chamber due to the accumulation of unburned mixture in crevices near the spark housing and the gas valve outlet. This issue is crucial when looking at vehicle emissions. Finally, the thermal quenching effect can affect the main pre-chamber operation. If the flame can propagate through the pre-chamber nozzles without quenching then the mixture in the cylinder is ignited by the jet flame front. On the contrary, if the flame is quenched within the nozzles, the mixture in the cylinder is ignited by hot radicals injected which create distributed combustion microkernels downstream of the nozzles. Modelling of these phenomena is essential to the successful design of PCI systems.

To simulate these effects, a novel phenomenological quenching model has been developed by Ricardo and implemented into the VECTIS CFD product to work with G-equation combustion model. This paper illustrates the principles and applications of the developed model. Following initial verification, the model is applied to the analysis of a novel pre-chamber ignition system developed within Horizon 2020 GASON project and the results are compared with measurement data.

Keywords

Quenching, flame-wall interaction, pre-chamber, lean burn, unburnt hydrocarbons, emissions.

Introduction

The interaction of the flame with the walls of the pre-chamber is an important issue affecting operation of the PCI combustion system in several ways. Firstly, the flame will quench near the wall due to heat losses [1-2]. This effect is more prominent in PCIs designed for light-duty vehicles in comparison to conventional ignition systems, as the characteristic size of PCIs can be not negligible compared to the flame quenching distance. Secondly, quenching affects the quality of the fuel mixture within the pre-chamber due to the accumulation of unburned mixture in crevices near the spark housing and the gas valve outlet. Finally, the thermal quenching effect can affect the mode of pre-chamber operation. When the flame can propagate through the pre-chamber nozzles, the mixture in the cylinder is ignited by the jet flame front [3-4]. On the other hand, when the flame is quenched within the nozzles, the mixture in the cylinder is ignited by hot radicals injected, which create distributed combustion microkernels downstream of the nozzles. Modelling of quenching is therefore essential to the successful design of PCIs.

It is accepted that quenching of a flame front in the vicinity of a solid wall is mainly controlled by heat losses, as demonstrated by DNS results [2] and by experimental measurements [5]. Heat losses to the walls are associated with a decrease in temperature at the flame front, which slows down the rate at which radicals are generated. Beyond a certain rate of heat loss, the flame cannot self-sustain and quenches. This threshold has been observed to be of the order of a third of the flame power.

The distance from the wall beyond which the flame front cannot keep propagating is referred to as the quenching distance, and it generally depends on parameters such as the fuel type, the equivalence ratio of the mixture, the local temperature and pressure, as well as on the characteristics of the wall itself [6].

Efforts have been taken towards reducing the number of independent parameters of the problem by means of dimensional analysis [1]. The quenching distance may be described in terms of a quenching Peclet number, which simplifies the formulation of a correlation directly applicable to quenching models.

The mechanism by which quenching effects can be incorporated into the combustion model is highly dependent on the latter. Once the actual local parameters of flame quenching are determined, the development of the quenching model for combustion models relying solely on the reaction source to propagate the flame is arguably straightforward. However, the application of quenching to combustion models which attempt to directly resolve the flame front propagation through both convection and reaction, such as flame surface density model [2] or the classical G-equation model is more difficult and, in the case of G-equation combustion model, has not been accomplished so far. The development of the model and the validation experiment is presented in the following sections.

Modelling methodology

The quenching approach has been developed based on the experimental correlation of the quenching Peclet number adopted after [1]:

$$Pe_q = \frac{\delta_Q}{\delta_f} \tag{1}$$

where δ_Q and δ_f are the quenching distance and the laminar flame thickness, respectively.

The quenching Peclet number is correlated to the experimental data of [1] as a function of pressure and equivalence ratio, resulting in the following expression for the two-plate quench distance depending on the equivalence ratio θ and pressure as follows:

$$Pe_2(1,\theta) = \begin{cases} 11.2e^{-2.13(\theta-0.8)}, & 0.7 < \theta \leq 0.8 \\ 9.9e^{-0.63(\theta-1.0)}, & 0.8 < \theta \leq 1.0 \\ 9.9, & 1.0 < \theta \leq 1.2 \\ 9.9e^{-0.30(\theta-1.2)}, & 1.2 < \theta \leq 1.5 \end{cases} \quad (3)$$

$$Pe_2(p,\theta) = \begin{cases} Pe(1,\theta), & p \leq 1atm \\ Pe(1,\theta)\left(\frac{Pe(3,\theta)}{Pe(1,\theta)}\right)^{\frac{p-1}{2}}, & 1atm < p \leq 3atm \\ \frac{9.5}{\theta}\left(\frac{p}{3}\right)^{0.26\min\left(1,\frac{1}{\theta^2}\right)}, & 3atm < p \leq 40atm \end{cases} \quad (4)$$

The head-on quenching Peclet number is then recovered from the two-wall quenching Peclet as:

$$Pe_Q = 0.5Pe_2 \quad (5)$$

A correction is adopted following [7] to account for wall heating:

$$Pe_Q = Pe_Q^{isothermal} \cdot \frac{T_{flame} - T_{wall}}{T_{flame} - T_{unburnt}} \quad (6)$$

The quenching factor for a cell is derived based on the ratio of the quenched mass to the mass of the cell:

$$\Phi_Q = \frac{m_Q}{m_{cell}} = \frac{\rho_u V_Q}{\rho_u V_Q + \rho_b (V_{cell} - V_Q)} \quad (7)$$

Where subscripts u and b refer to unburnt and burnt mixture respectively and V_Q is the quenched volume expressed by projecting wall patches by δ_Q along wall patch normal. The transition between the fully quenched layer and the layer unaffected by quenching is done linearly up to the influence layer distance δ_Q calculated at $Pe_Q^{isothermal} = 10$ (see [2]).

To incorporate the quenching factor into the G-equation combustion model, an approach is adopted similar to the one proposed for the flame surface density combustion model by Poinsot et al. [2]. A source term is introduced in the G-scalar transport equation designed to suppress both convective and burning mechanisms of the flame front propagation in the quenched zone. The resulting modified G-equation model is formulated as follows:

$$\frac{\partial \tilde{G}}{\partial t} + \vec{U} \cdot \nabla \tilde{G} = S_p \left|\nabla \tilde{G}\right| + S_Q \quad (9)$$

Where S_p is the local flame propagation speed and the quenching source term takes the following form:

$$S_Q = -\Phi_Q \cdot \left[-U \cdot \nabla \tilde{G} + S_p \left|\nabla \tilde{G}\right|\right] \quad (10)$$

The term tends to zero outside the quenching layer and fully negates the convection and burning propagation of the G-scalar within the fully quenched zone. Verification tests have been conducted on a simple bomb geometry with an added cavity to ensure that the flame does not propagate into cavities of width less than the quenching distance under given conditions.

Experimental methodology

The RCEM operates in a single cycle mode (compression-expansion), and combines excellent optical access with high flexibility in independently changing parameters such as mixture composition, start of ignition, filling pressure, etc. A detailed description of the principle of operation of the RCEM together with the list of the most important specifications of the machine can be found in [8]. In brief, the experimental section of the RCEM consists of the cylinder head with the PC centrally mounted, the combustion chamber and the working piston with the quartz window. The bore and the quartz piston diameter are B=84mm and D=52mm, respectively. A UV-enhanced mirror is placed behind the quartz piston in order to allow the detection of the reacting jets exiting, the ignition and the combustion inside the MC. For this purpose, the high speed 2D OH* chemiluminescence imaging was performed using an intensified high speed camera at 32 kHz repetition rate (LaVision HSSX and image intensifier, 10/12 bits dynamic range) equipped with a 50 mm UV lens (f/2.0) and a bandpass filter for a wavelength of 306 nm and 12.1 nm FWHM. In order to extract information about the jet exiting time and its morphology, a purpose-built Matlab routine was employed. By using this routine, firstly the OH* image was divided into 7 sub-areas, covering the area in front of a single nozzle. The total pixels` intensity of each sub-area was integrated for each frame, for all 600 frames covering the combustion event. The user was able then to define an intensity threshold suitable for each case to capture accurately the time of emergence of each jet in the main chamber. This threshold was introduced to avoid misinterpreting image noise as reactive jet. By this means, the jet exiting time for the first jet was defined.

The jets were formed by a GASON PC-A pre-chamber prototype with the inner volume of 1.826cm^3 and 7 orifices of 1.5mm diameter each. The orientation of the orifices was tangential to the pre-chamber cross-section, to create a swirling motion of the incoming mixture during compression. A schematic of the pre-chamber and the numbering of nozzles is illustrated in Fig. 1.

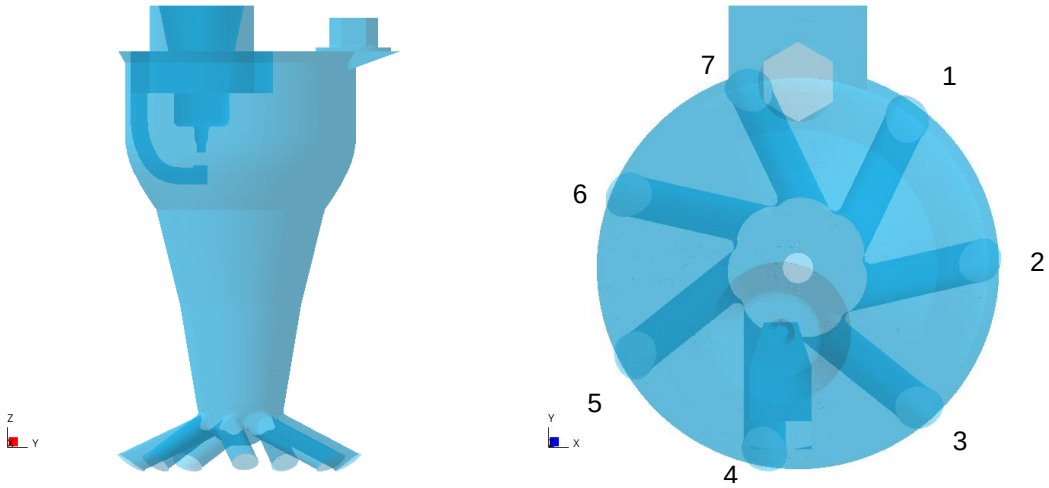

Figure 1: Schematic of the PC-A pre-chamber geometry.

The piston stroke was set at 250mm and the temperature of the cylinder head and liner was set at 383K. The initial pressure inside the combustion chamber was 1.2 bar. Additional piezo-resistive pressure sensors were mounted on the driving piston and the fuel supply line of the PC and MC to control the filling of the driving gas (set at 27bar), and the fuel pressure (set at 10 bar for the PC and set at 60 bar for the MC). The fuel for the filling of the MC was administered by a Siemens hollow cone piezo injector and for the PC by a prototype injector (Bosch system NG12). To achieve a homogeneous

background methane-air mixture, the methane was injected into the chamber about 3s bTDC and prior to the start of compression. Contrary to a real engine, no turbulence exists in the MC at the beginning of the stroke. The start of fuel injection in the PC was performed during the compression, when the pressure of the main chamber was 2.0 bar. The fuel for the MC and PC was supplied from high purity methane bottles (99.995% CH4). The ignition was initiated by an ignition coil (VW AG 06.J.905.110.G, BEO S3) with a G-type spark plug, which has a 0.5mm gap. The pressure at start of ignition was kept constant for all measurements at 26bar. The synchronisation of all trigger events, namely the start of injection in the PC and MC, the ignition timing and the simultaneous camera recording trigger signal, was achieved using a pressure and a position-based system at certain cylinder pressures and piston positions. The nomenclature and conditions for the cases investigated are summarized in Table 1. Injection duration into the pre-chamber of 2.5ms was used in all cases. The mass flow rate for the main part of injection into the pre-chamber was estimated to be 4.0e-4 kg/s.

Case	Pressure at BDC Bar	Main Charge λ	Injection timing ms bTDC	Spark timing ms bTDC
L001_006	1.400	1.6	21.9	2.96
L002_002	1.375	1.8	21.9	3.03
L003_004	1.387	2.0	22.06	2.92

Table 1: Cases and corresponding conditions.

CFD analysis

The evaluation of the early flame development in the pre-chamber mounted on an RCEM has been performed for the baseline GASON pre-chamber model PC-A. The comparisons are focussing on the effect of quenching on flame propagation as measured in the experimental set-up by the delay between the ignition timing and appearance of the flame front at the nozzle as observed through the optical access window at the flat portion of the piston.

Gas injection into the pre-chamber was modelled using flat injection profile with 0.5ms linear valve opening and closing intervals. Following a mesh dependency study, cartesian mesh with basic cell size of 0.18mm and two levels of refinement towards the walls was used for all reported simulation. Simulation settings and models used are summarised in Table 2.

Model/parameter	Value
Spark model	Dynamic DPIK [9]
Breakdown energy	0.1mJ
Effective power	180W
Spark duration	1.8ms
1D/3D transition radius	4mm
Laminar flame speed	Metghalchi & Keck [10]
Turbulent flame speed	Herweg and Maly (w/o strain correction [11])
Flame speed multiplier	3.0
Initialisation	Quiescent, test data at 37 ms bTDC

Table 2: Simulation settings.

Fig. 2 illustrates the distribution of the equivalence ratio in the symmetry plane of the spark plug and in the vertical plane passing through the centre of the spark plug gap for case L002_002 at ignition time

t=-3.03ms (with zero time level corresponding to TDC). The complex flow pattern with the spiral vortex attached to the walls of the pre-chamber driven by the nozzle flow in the compression stroke results in a highly non-uniform distribution of the injected fuel. The conditions are particularly rich at the top of the pre-chamber, where the injected fuel is trapped in the spark plug case gap and near the gas valve opening. However, the fuelling strategy succeeds in achieving optimal conditions close to stoichiometry at the location of the spark centroid.

Fig. 3 illustrates the spatial distribution of the quenching factor at the time of ignition for the same case. The model predicts partial quenching occurring in the nozzles and in the areas at the top of the pre-chamber which corresponds to rich conditions of trapped fuel. However, in the pre-chamber core, the quenching layer at the walls is very thin and is unlikely to have a significant effect on the flame propagation.

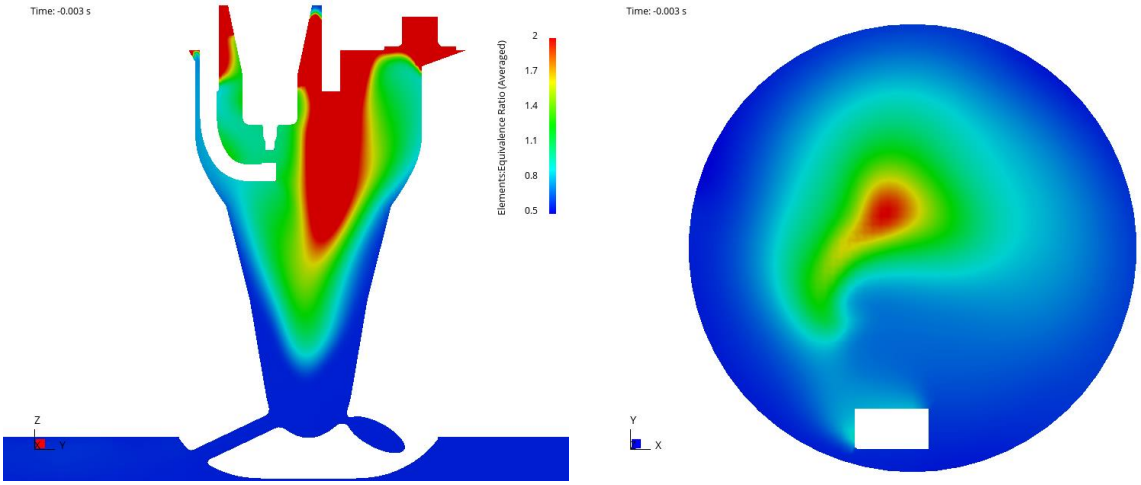

Figure 2: Equivalence ratio distribution at the point of ignition in the spark plug symmetry plane (ZX, left) and an XY plane through the centre of the spark gap (right).

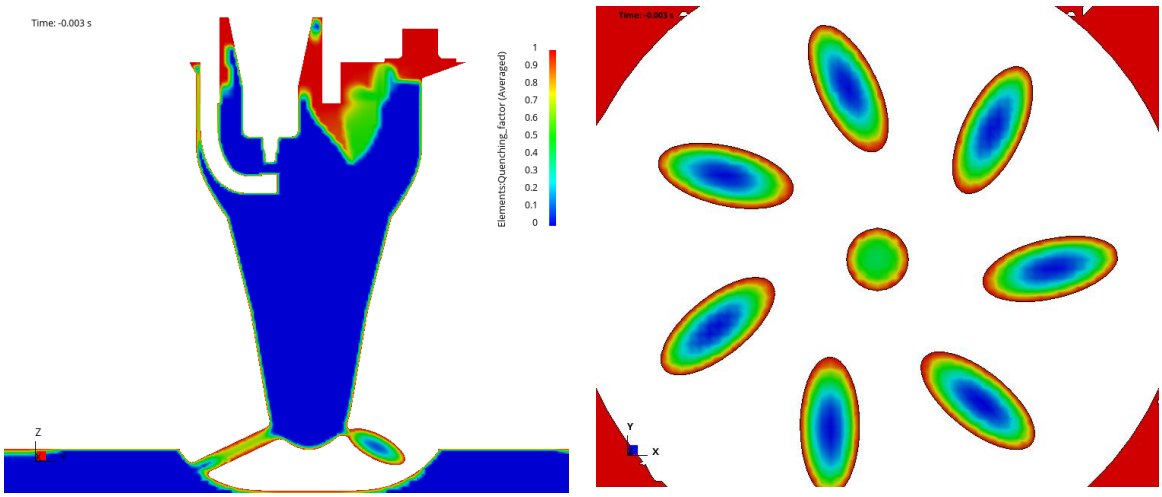

Figure 3: Quenching factor distribution at the point of ignition in the spark plug symmetry plane (ZX, left) and in a Z slice through the nozzles in the flame face plane (right).

To enable quantitative comparison of the effects of quenching with the experimental data, surface sensors were introduced in the CFD simulation covering the outlets of the pre-chamber nozzles on the cylinder side (see also Fig. 1). Fig. 4 illustrates surface average fraction of the burnt fuel in the mass flow passing through the nozzle for all nozzles. The results indicate that while there is a substantial difference in the composition of the burnt mixture passing through the nozzles, the flame front reaches the nozzles almost simultaneously, resulting in a symmetric propagation of the flame front inside the cylinder. As expected, wall flame quenching delays the propagation of the flame but the effect is very limited.

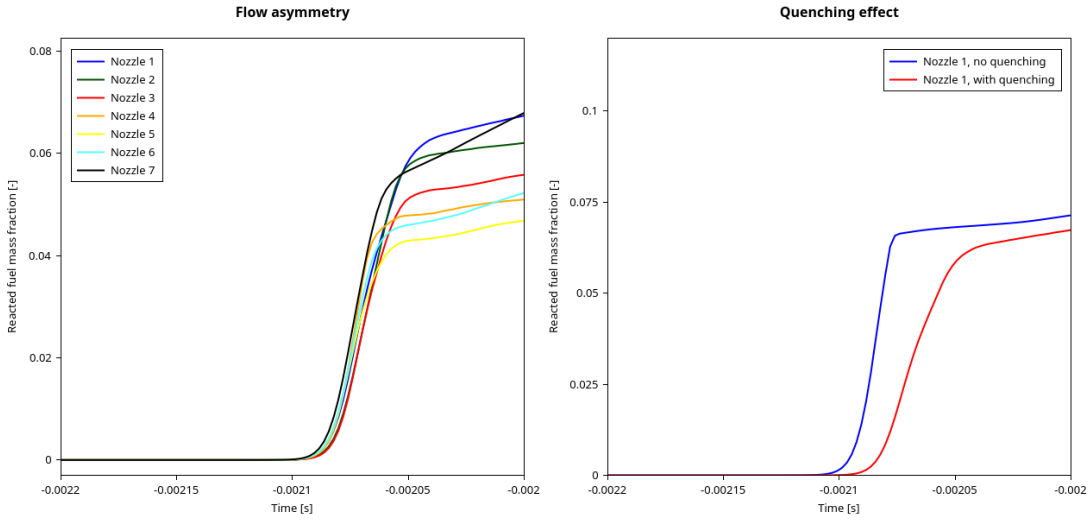

Figure 4: Burnt fuel mass flow through nozzles with quenching model applied (left) and comparison of quenching effect (right).

The exit time of flame jets has been estimated by comparing the average point in time at which the mass fraction of burnt fuel reaches 1.e-3 at the nozzle exit, the threshold was selected based best fit for results across the range of simulated cases. The results obtained with this criterion are summarised in Table 3. In all cases, the quenching model delays the propagation of the flame however the quantitative difference in the results is well within the accuracy of the definition of the flame front position. Quenching model yields a better prediction for rich conditions, whereas for lean conditions quenching simulation deviates further from the experiment. In all simulated cases, the zero level of G-scalar representing the flame front position propagates through the nozzles without quenching. The experimental observations confirm this prediction.

Case	Test	Simulation	Simulation with quenching
L001_006	0.95	0.925	0.936
L002_002	0.90	0.930	0.942
L003_004	0.97	0.975	0.988

Table 3: Flame jet exit time in ms.

Conclusions

A quenching model has been developed within the context of G-equation combustion model. The model is based on an experimental correlation from [1] with a wide range of applicability, augmented to account for the walls temperature effects and finite width of the quenching layer following DNS data of [2]. The resulting formulation is compact and fast to evaluate, the main computational expense is associated with the computation of wall distance. The model has been validated with respect to the original correlation of [1] and then evaluated in comparison with the experimental data obtained for an RCEM-mounted pre-chamber. CFD results indicate absence of full quenching in pre-chamber nozzles and the flame propagation times agree well with the experimental observations confirming that pre-chamber operates in the desired flame torch mode.

This work has been supported by the Horizon 2020 GASON project, Grant agreement number 652816.

References

[1] **Lavoie, G.** *Correlations of combustion data for s.i. engine calculations - laminar flame speed, quench distance and global reaction rates.* SAE Technical Paper (1978), 780229.

[2] **Poinsot, T. J., Haworth, D. C. and G. Bruneaux, G.** *Direct Simulation and Modeling of Flame-Wall Interaction for Premixed Turbulent Combustion.* Combustion and Flame 95 (1993) 118-132.

[3] **Toulson, E., Schock, H.J. and Attard, W. P.** *A review of pre-chamber initiated jet ignition combustion systems.* SAE International (2010), 2010-01-2263.

[4] **Sadanandan, R., Markus, D., Schiessl, R., Maas, U., Olofsson, J., Seyfried, H., Richter, M. and Alden, M.** *Detailed investigation of ignition by hot gas jets.* Proceedings of the Combustion Institute 31 (2007) 719-726.

[5] **Boust, B., Sotton, J., Labuda, S. A. and Bellenoue, M.** *A thermal formulation for single-wall quenching of transient laminar flames.* Combustion and Flame 149 (2007) 286-294.

[6] **Bellenoue, M, Kageyama, T., Labuda, S. A. and Sotton, J.** *Direct measurement of laminar flame quenching distance in a closed vessel.* Experimental Thermal and Fluid Science 27 (2003) 323-331.

[7] **Bellenoue, M, Boust, B, Bernard, L., Sotton, J. and Labuda, S.A.** *A model for flame quenching in non-isothermal initial conditions.* Proceedings of the European Combustion Meeting, Vienna (2009).

[8] **Schlatter, S., Schneider, B., Wright, Y., Boulouchos, K.** *Experimental Study of Ignition and Combustion Characteristics of a Diesel Pilot Spray in a Lean Premixed Methane/Air Charge using a Rapid Compression Expansion Machine.* SAE International (2012), 2012-01-0825.

[9] **Tallu, G., Beck, L. M., Prouvier, M. , Winkler, A., Frambourg, N. and Shapiro, E.** *3D CFD modelling and simulation of spark ignition inclusive of turbulence effects and detailed chemical kinetics.* Proceedings of the 3rd Internation Conference on Ignition Systems for Gasoline Engines, Berlin (2016).

[10] **Metghalchi, M. and Keck, J. C.** *Burning velocities of mixtures of air with methanol, iso-octane and indolene at high pressure and temperature.* Combustion and Flame 44 (1982) 1081-1093.

[11] **Herweg, R. and Maly, R. R.** *A fundamental model for flame kernel formation in S.I. engines.* SAE International (1992), 922243.